NANO LETTERS

Letter

pubs.acs.org/NanoLett

Photon Cascade from a Single Crystal Phase Nanowire Quantum Dot

Maaike Bouwes Bavinck,[†] Klaus D. Jöns,[†] Michal Zieliński,[‡] Gilles Patriarche,[§] Jean-Christophe Harmand,[§] Nika Akopian,*[,∥] and Val Zwiller[†,⊥]

[†]Kavli Institute of Nanoscience, Delft University of Technology, 2600 GA Delft, The Netherlands

[‡]Instytut Fizyki, UMK, Grudziądzka 5, Toruń 87-100, Poland

[§]Laboratoire de Photonique et de Nanostructures, CNRS, route de Nozay, 91460 Marcoussis, France

[∥]Department of Photonics Engineering, Technical University of Denmark, 2800 Kongens Lyngby, Denmark

[⊥]Department of Applied Physics, KTH Royal Institute of Technology, SE-100 44, Stockholm, Sweden

Supporting Information

ABSTRACT: We report the first comprehensive experimental and theoretical study of the optical properties of single crystal phase quantum dots in InP nanowires. Crystal phase quantum dots are defined by a transition in the crystallographic lattice between zinc blende and wurtzite segments and therefore offer unprecedented potential to be controlled with atomic layer accuracy without random alloying. We show for the first time that crystal phase quantum dots are a source of pure single-photons and cascaded photon-pairs from type II transitions with excellent optical properties in terms of intensity and line width. We notice that the emission spectra consist often of two peaks close in energy, which we explain with a comprehensive theory showing that the symmetry of the system plays a crucial role for the hole levels forming hybridized orbitals. Our results state that crystal phase quantum dots have promising quantum optical properties for single photon application and quantum optics.

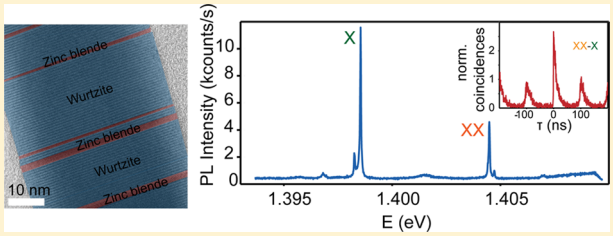

KEYWORDS: *Crystal phase quantum dot, nanowire, InP, two-photon cascaded emission, type II transition*

Controlling the confinement of charge carriers in semiconductors at the nanoscale is at the heart of optoelectronics. Confinement is generally realized with heterostructures and has led to zero dimensional quantum devices operating at the single electron and photon level. In particular, single and entangled photon sources have been developed with semiconductor heterostructures.[1−7] Tailoring the optical properties of these artificial atoms and designing complex devices still remain one of the main challenges for such structures due to the self-assembled growth process. This process inhibits the precise control of the geometry and composition. However, crystal phase quantum dots, also called polytype nanodots,[8] offer a promising solution, because crystal phase quantum dots are defined by a modification in the crystallographic structure of a nanowire, unlike the commonly used change in material composition. The crystalographic structures do not intermix within a monolayer and thus always have atomically sharp interfaces, allowing for the geometry control with the precision of a single atomic layer. A switch between a zinc blende (cubic lattice) and a wurtzite (hexagonal lattice) section defines a confining potential, because the crystal phases have different band structures.[9,10] For example, GaP and Ge have an indirect bandgap in the zinc blende structure but are predicted to have a direct character in the wurtzite structure.[11,12]

In bulk, different crystal structures rarely coexist,[13] however, in nanowires they easily form during growth and remain metastable under ambient conditions[14] due to the monatomic layer nucleation stage.[15,16] For example, bulk InP is found in the zinc blende lattice, while an InP nanowire can be grown in either zinc blende or wurtzite lattices with possible coexistence of both structures.[17] A zinc blende segment surrounded by wurtzite InP can confine electrons and form a crystal phase quantum dot.[17] A great advantage of such a system is that the interface of the quantum dot is intrinsically sharp down to the atomic level.[8,18] This enables higher control compared to self-assembled quantum dots where alloying blurs interfaces, implying that quantum dots' heights and intervals can be controlled with atomic layer accuracy,[18] an unprecedented degree of control. Such high control has been shown in InAs[18] and GaP[20] nanowires, where the height of zinc blende and wurtzite segments is controlled, however, the control of the crystal structure of InP is still a challenge.

Such systems are relevant for quantum information, where each crystal phase quantum dot confining a charge can be operated as a qubit to form a quantum register in a single nanowire. Most importantly, this type of quantum dot is useful in quantum optics for generation of single and two photon states, as shown in this work. Precise control of the crystal

Received: October 16, 2015
Revised: January 13, 2016
Published: January 25, 2016

DOI: 10.1021/acs.nanolett.5b04217
Nano Lett. 2016, 16, 1081−1085

phase in nanowires therefore represents a major opportunity for materials at the nanoscale.

In InP, electrons are confined in zinc blende and holes in wurtzite[19] leading to indirect transitions between different crystal structures, referred to as type II transitions. In general, type II quantum dots have shown interesting physics, such as the Aharanov-Bohm effect,[21,22] excitonic Mott transitions,[23] and applications to solar cells[24,25] and photon-detectors.[26,27] Whereas all of these studies have been performed on ensembles, here we study quantum emitter properties of a single type II quantum dot. These have been difficult to observe as emission intensities are generally far weaker than from type I quantum dots due to a small overlap of electron and hole wave functions. These challenges are addressed in this Letter, where we show that type II crystal phase quantum dots in InP have excellent properties in terms of emission line width and brightness. The spectra are comprehensively explained by tight binding calculations showing hole levels of molecular-like character, very different from the single particle level in type I quantum dots. Moreover, we report a two-photon quantum cascade from correlation measurements on type II quantum dots, a crucial prerequisite to generate entangled photons.[28]

We study wurtzite InP nanowires with base diameters ranging from 110 to 160 nm, tapered toward the top (Figure 1a). The sample was grown on (111)B InP using Au-catalyzed

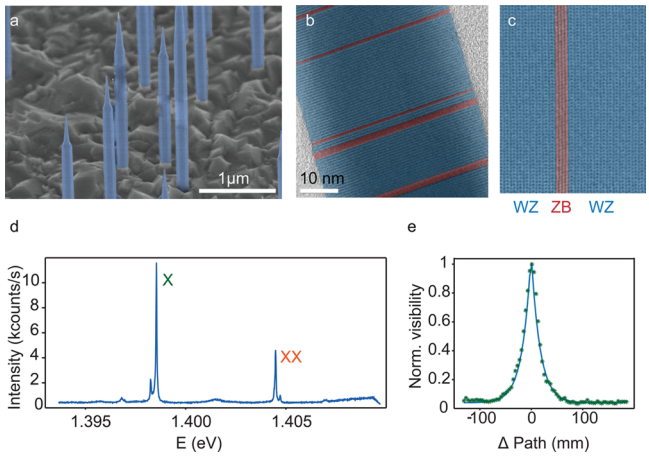

Figure 1. (a) Scanning electron microscope image of the as-grown InP nanowire sample. (b) Transmission electron microscopy of InP nanowires showing short segments of zinc blende (red) in a wurtzite (blue) nanowire. (c) A high resolution-transmission electron microscopy image of the zinc blende segment in the otherwise wurtzite lattice. (d) μ-photoluminescence spectra from a crystal phase quantum dot and (e) Michelson Fourier spectroscopy of the line labeled X in panel d. From the envelope, we extract a Lorentzian line width of 23 ± 1 μeV.

vapor−liquid−solid synthesis by molecular beam epitaxy. The initial growth at 420 °C favors the wurtzite phase and was gradually decreased to 380 °C to produce short zinc blende insertions[29] with an average density of 15 segments/μm, causing each wurtzite/zincblende/wurtzite quantum dot system to have a total length of 60 nm on average.

The nanowires are studied in a μ-photoluminescence bath cryostat setup at 4.2 K using a 0.85 numerical aperture objective. Photoluminescence measurements were performed using a continuous laser at 532 nm. The photoluminescence signal was sent to a spectrometer with resolution of 30 μeV and detected with a CCD-camera. The line width is extracted from a coherence measurement using a Michelson interferometer. For the Hanbury Brown and Twiss experiment, we used a pulsed laser diode (wavelength of 640 nm, pulse length <100 ps) at a repetition rate of 5 MHz. The photoluminescence signal was spectrally filtered by a spectrometer and correlation measurements were performed using two avalanche photodiodes (80 darkcounts/s, time resolution of 450 ps). For all measurements the laser spot size was ∼1 μm in diameter.

Figure 1b shows that the length of the wurtzite segments differ, breaking the symmetry around each zinc blende section. This high-resolution transmission electron microscope image shows that the heights of the zinc blende sections vary within a couple of monolayers. Atomically sharp transitions (Figure 1c) between the zinc blende and wurtzite phases are observed. For optical studies, single nanowires were transferred to a silicon-on-insulator wafer.

In Figure 1d, a microphotoluminescence spectrum of a single crystal phase quantum dot shows bright emission with comparable intensities to type I quantum dots (measured in the same setup[30]) and strong polarization along the nanowire growth z-axis (Supporting Information Figure S1). We measure the coherence length under above-band excitation for line X in a Michelson interferometer and extract from an exponential fit a line width of 23 ± 1 μeV. This narrow line width is remarkable as indirect excitonic transitions (type II) typically have a broader line width (>200 μeV).[31,32] We suggest that this narrow line width originates from the weakly confined hole states, which is typically a continuum of states for type II systems. Because of the weak localization, the interaction with the environment is limited compared to a continuum of states. The transitions X and XX consist of two lines of different intensities with respective splittings of 240 ± 30 and 220 ± 30 μeV, which we explain with atomistic calculations. Several spectra from additional crystal phase quantum dots are shown in Supporting Information Figure S2.

Figure 2a sketches the bandstructure of an InP zinc blende quantum dot in a wurtzite matrix. InP wurtzite has a wider bandgap (1.474 eV) than zinc blende (1.410 eV) and the zinc blende conduction band was calculated to be 129 meV below the wurtzite conduction band.[19] We use empirical tight-binding calculations for electron and hole states with an sp3s* orbital and nearest-neighbors coupling. The single particle configuration is then followed by a many-body calculation. (Supporting Information S3). We model the crystal phase quantum dot as an InP zinc blende segment of length $(ZB)_n$ embedded between two wurtzite segments of $(WZ)_m$, where n and m refer to the number of layers. We consider diameters from 6 to 48 nm and a total length longer than 60 nm (∼200 monolayers), corresponding to the average wurtzite/zinc blende/wurtzite length determined from transmission electron microscopy.

Figure 2b shows probability densities for the ground electron state (e_0) and the first optically (z-polarized) active hole state (h_2) for a $(ZB)_4$ quantum dot. The confined electron state energy separation is comparable with well-known quantum dot systems such as InAsP quantum dots (Supporting Information S4). In contrast to well-confined hole states in traditional quantum dots, hole states in crystal phase quantum dots are weakly localized with energy spacing between subsequent levels below 1 meV. For this system (Figure 2b), 80% of the electrons are localized in the zinc blende, while the probability to find the hole in zincblende section is only 0.1%. Hole states in both

DOI: 10.1021/acs.nanolett.5b04217
Nano Lett. 2016, 16, 1081−1085

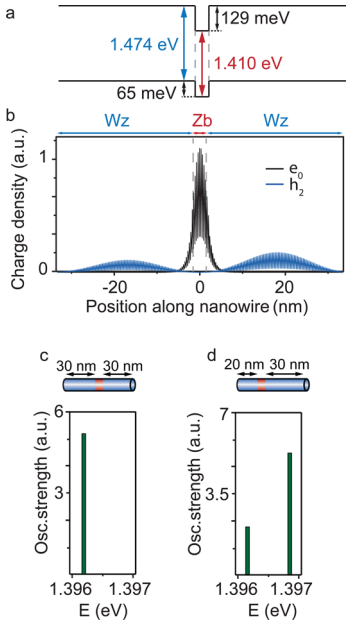

Figure 2. Tight-binding calculations of a zinc blende section in a wurtzite nanowire. (a) Calculated band alignment used in our calculations. (b) Probability density of the ground electron state (e_0) and the second excited hole state (h_2), calculated along the growth direction of the nanowire for a $(ZB)_4$ crystal phase quantum dot. The gray dashed lines mark the zinc blende–wurtzite (ZB–WZ) interfaces. The apparent fringes on density plots are related to charge oscillations between subsequent anion/cation layers. The electron localization within the zinc blende section reaches 80%, whereas the probability to find the hole in the zinc blende section is only about 0.1%. In panels c and d, the s-shell spectra calculated for a zinc blende section of $(ZB)_4$ surrounded by (c) two symmetric wurtzite and (d) a reduced symmetry between the wurtzite segments is shown. The broken symmetry splits the ground level of the exciton. All calculations were obtained for a nanowire diameter of 48 nm.

wurtzite sections couple through the zinc blende and split into hybridized states. In small diameter nanowires, hole states are separated by tens of microelectronvolts. However, for larger diameter systems (>48 nm) the energy spacing is reduced such that a simplified single particle picture must be replaced by a many-body approach accounting for configuration mixing. Large diameter crystal phase quantum dots constitute therefore a highly correlated system.

For different $(ZB)_n$ stackings, the oscillator strengths in a 48 nm diameter nanowire are calculated to estimate the height of our measured crystal phase quantum dots. We find that a quantum dot of height $(ZB)_4$, embedded between two symmetric wurtzite segments of 30 nm height (symmetric case), has an optically active transition at ∼1.4 eV, which is in good agreement with the experimental findings in Figure 1d. From transmission electron microscopy (Figure 1b), we observe that wurtzite segments have a length distribution.[16] We therefore perform calculations for systems where left and right wurtzite segments have different lengths and one side is shortened to 20 nm (asymmetric system). Although this does not influence the well-confined electronic states in the zinc blende, the weakly localized hole states are sensitive to such symmetry changes. Figure 2c,d depicts the calculated spectra for symmetric and asymmetric cases, where only polarizations along the nanowire growth direction (z-polarized) are shown. Only this polarization from the quantum dot is detectable from the side due to the nanowire geometry and the dielectric mismatch between the nanowire and the environment.[33,34] For completeness, the x/y-polarized transitions, not observed in our experiments, are given in the Supporting Information (Figure S4).

The calculated symmetric case spectrum (Figure 2c) shows a single exciton peak, stemming from excitonic configurations involving predominantly second (h_2) and third excited hole states (h_3). Configurations involving the ground hole (h_0) and first excited hole state (h_1) reveal only very weak z-polarized optical activity and are not visible.

For the asymmetric system (Figure 2d), we find not one but two z-polarized lines separated by 700 ± 30 μeV. This splitting does not originate from anisotropic exchange interactions[35] but from the hybridized character of the hole states: the first excited hole state (h_1) has now an optically allowed transition with a s-shell electron. The lower energy line originates from a hole in the second excited state (h_2), whereas the transition with the ground hole state remains dark. This corresponds well to the double peaks in our experiments (Figure 1d). We perform calculations for different geometries and find that the spectra strongly depend on the zinc blende section length and on the wurtzite matrix asymmetry. Our calculations predict that a higher symmetry wurtzite matrix results in a single z-polarized peak, whereas asymmetry leads to two z-polarized transitions (Supporting Information Figure S4). Typical measurements of the photoluminescence spectrum show a dominant line with a side peak for exciton and biexciton complexes separated by 70–240 μeV with varying intensity ratio. We conclude from our calculations that the splitting of the measured lines in Figure 1d originates from an asymmetry in the wurtzite matrix.

Additionally, we calculate the spectra of the exciton (X) and biexciton (XX) for a $(ZB)_1$ system. By reducing the zinc blende section length, electron confinement increases resulting in higher excitonic emission energies ($E_x \sim 1.46$ eV). Figure 3a shows calculations of z-polarized exciton and biexciton oscillator strengths for a $(ZB)_1$ section between 34 and 30 nm wurtzite segments, predicting a double peak for the exciton and four lines for the biexciton. We calculate a binding energy ($E_{xx-x} = E_{xx} - E_x$) of 2.7 meV resulting in an unbound biexciton.

Figure 3b presents the measured power series of a single crystal phase quantum dot, matching the calculated spectra for the $(ZB)_1$ system. The spectra show the typical power dependence of a biexciton–exciton cascade.[36] From our measurement, we find that the exciton (biexciton) complex consist of two peaks split by 100 ± 30 μeV (90 ± 30 μeV). The biexciton binding energy of this quantum dot is 2.7 meV, which is in excellent agreement with our calculations for $(ZB)_1$ systems. The calculations for different $(ZB)_n$ systems typically give an unbound biexciton ($E_{xx-x} > 0$) with binding energies ranging from 1.5 to 12 meV, confirmed by our experiments (2–6 meV). From the single configuration (Hartree–Fock) picture, the positive binding energy is intuitively understood by the weak Coulomb interactions between electrons and holes and the strong electron–electron repulsion.

We measure the polarization in six different bases (horizontal, vertical, diagonal, antidiagonal, and left and right circular) and analyze the data calculating Stokes parameters. The parameters can then be parametrized and plotted, as shown in Figure 3c,d for the exciton and biexciton, respectively. In the plot, also the direction of the nanowire compared with

DOI: 10.1021/acs.nanolett.5b04217
Nano Lett. 2016, 16, 1081–1085

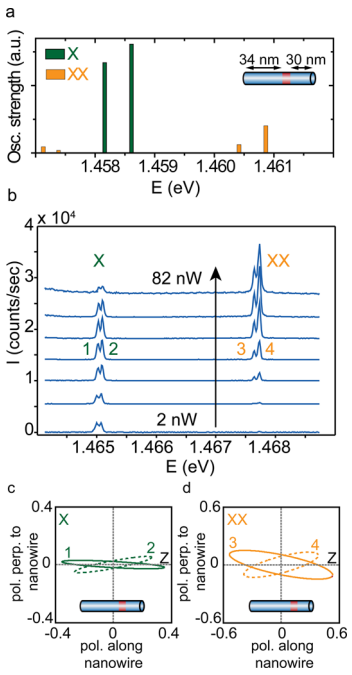

Figure 3. (a) Calculations for the exciton (X) and biexciton (XX) for a zinc blende embedded between two wurtzite sections of 34 and 30 nm. (b) Power-dependent photoluminescence spectra of a crystal phase quantum dot. At low power, we observe a single split peak (1,2) and with increasing power, we observe a second double peak (3,4), that we relate respectively to an exiton and a biexciton. The excitonic (c) and biexcitonic (d) transitions are polarized along the nanowire (Z), which is in agreement with our calculations. The dotted lines in both figures correspond to the peaks at higher energy.

the polarization is given, showing that the lines are *z*-polarized along the nanowire, confirming our theoretical calculations.

Figure 4a depicts autocorrelation measurements on the exciton (X of Figure 1d) with clear antibunching, demonstrat-

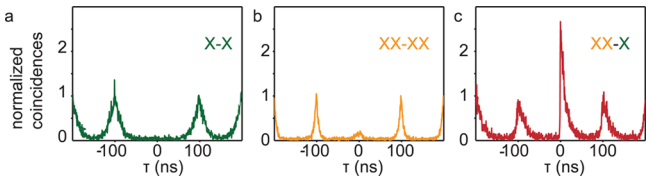

Figure 4. Autocorrelations showing antibunching for (a) exciton and (b) biexciton of the lines labeled X and XX in Figure 1d. (c) Cross-correlations between the exciton (X) and biexciton (XX) line. The asymmetric correlation peak at zero time delay shows clear bunching (antibunching) for positive (negative) time delays, the proof of a two-photon cascade.

ing pure single-photon emission. For the biexciton (XX) (Figure 4b), we extract from an exponential fit a $g^{(2)}(0)$ of 0.15 ± 0.02, caused by an increased background signal or re-excitation at higher excitation power. We find the lifetimes for the exciton and biexciton to be 10.59 ± 0.63 and 4.63 ± 0.45 ns respectively (lifetime ratio of ∼2.3) (Supporting Information Figure S5). These long lifetimes result from the reduced wave function overlap in type II systems. For different crystal phase quantum dots, we measure lifetimes in the range of 4−90 ns, controlled by the nanostructure geometry.[37]

Cross-correlation experiments in Figure 4c, where the biexciton photon triggers the start and the measurement stops on an exciton detection, show clear bunching (antibunching) for positive (negative) time delays: the confirmation of a two-photon cascade. The two-photon cascade in type I quantum dots enables generation of polarization-entangled[1−6] and time-bin entangled photon-pairs.[7] Our demonstration of this cascade in crystal phase quantum dots is an important step toward new applications for crystal phase nanostructures as quantum state emitters, because theory predicts an excitonic finestructure splitting of zero for systems with C_{3v} symmetry[38,39] and entanglement has been shown from quantum dots with such symmetry.[5]

Our results show that a change in the crystal structure within the same material can give rise to pure single photons of excellent quantum optical properties, demonstrating crystal phase quantum dots are a new type of excellent single photon emitters. The reported cascaded photon emission opens up the possibility to generate single and entangled photons from spatially separated electron−hole pairs. Our comprehensive theory, used to extract geometrical parameters, correctly predicts and explains our experimental findings and allows for future design of advanced crystallographic structures. This concept of crystal phase quantum confinement applies to material systems beyond III/V semiconductors.[40,41] Our measurements and calculations show that crystal phase quantum dots are not only a promising system due to their excellent optical properties but also contain rich physics that can be accessed and engineered by controlling the growth.

■ ASSOCIATED CONTENT

Supporting Information

The Supporting Information is available free of charge on the ACS Publications website at DOI: 10.1021/acs.nanolett.5b04217.

Polarization for the optical transitions of Figure 1d, additional spectra, methods for the theoretical calculations, calculated electron−hole states, calculations showing *z* and *x*/*y* transitions for different systems, and fits for extraction of lifetime. (PDF)

■ AUTHOR INFORMATION

Corresponding Author

*E-mail: nikaak@fotonik.dtu.dk.

Author Contributions

M.B.B., K.D.J., and M.Z. contributed equally.

The manuscript was written through contributions of all authors. All authors have given approval to the final version of the manuscript.

Funding

The research leading to these results has received funding from the European Research Council under the European Union's Seventh Framework Programme (FP/2007−2013)/ERC Grant Agreement n. [307687]. It was supported by NanoNextNL of the Government of The Netherlands and 130 partners and by the Polish Ministry of Science and Higher Education as a research project No IP 2012064572 (Iuventus Plus). This work is part of the research program of the Foundation for Fundamental Research on Matter (FOM), which is part of The Netherlands Organisation for Scientific Research (NWO).

Notes

The authors declare no competing financial interest.

DOI: 10.1021/acs.nanolett.5b04217
Nano Lett. 2016, 16, 1081−1085

REFERENCES

(1) Akopian, N.; Lindner, N.; Poem, E.; Berlatzky, Y.; Avron, J.; et al. Entangled photon pairs from semiconductor quantum dots. *Phys. Rev. Lett.* **2006**, *96*, 130501.

(2) Young, R. J.; Stevenson, R. M.; Atkinson, P.; Cooper, K.; Ritchie, D. A.; et al. Improved fidelity of triggered entangled photons from single quantum dots. *New J. Phys.* **2006**, *8*, 29; *New J. Phys.* **2006**, *8*, 29.

(3) Hafenbrak, R.; Ulrich, S. M.; Michler, P.; Wang, L.; Rastelli, A.; et al. Triggered polarization-entangled photon pairs from a single quantum dot up to 30 K. *New J. Phys.* **2007**, *9*, 315.

(4) Juska, G.; Dimastrodonato, V.; Mereni, L. O.; Gocalinska, A.; Pelucchi, E. Towards quantum-dot arrays of entangled photon emitters. *Nat. Photonics* **2013**, *7*, 527−531.

(5) Kuroda, T.; Mano, T.; Ha, N.; Nakajima, H.; Kumano, H.; et al. Symmetric quantum dots as efficient sources of highly entangled photons: Violation of Bell ' s inequality without spectral and temporal filtering. *Phys. Rev. B: Condens. Matter Mater. Phys.* **2013**, *88*, 041306.

(6) Versteegh, M. A. M.; Reimer, M. E.; Jöns, K. D.; Dalacu, D.; Poole, P. J.; et al. *Nat. Commun.* **2014**, *5*, 5298.

(7) Jayakumar, H.; Predojević, A.; Kauten, T.; Huber, T.; Solomon, G. S.; et al. Time-bin entangled photons from a quantum dot. *Nat. Commun.* **2014**, *5*, 4251.

(8) Vainorius, N.; Lehmann, S.; Jacobsson, D.; Samuelson, L.; Dick, K. A.; et al. Confinement in thickness-controlled GaAs polytype nanodots. *Nano Lett.* **2015**, *15*, 2652−2656.

(9) Akopian, N.; Patriarche, G.; Liu, L.; Harmand, J.-C.; Zwiller, V. Crystal phase quantum dots. *Nano Lett.* **2010**, *10*, 1198−1201.

(10) Loitsch, B.; Winnerl, J.; Grimaldi, G.; Wierzbowski, J.; Rudolph, D.; et al. Crystal Phase Quantum Dots in the Ultrathin Core of GaAs−AlGaAs Core−Shell Nanowires. *Nano Lett.* **2015**, *15*, 7544.

(11) Assali, S.; Zardo, I.; Plissard, S.; Kriegner, D.; Verheijen, M. A.; et al. Direct band gap wurtzite gallium phosphide nanowires. *Nano Lett.* **2013**, *13*, 1559−1563.

(12) Wang, S. Q.; Ye, H. Q. First-principles study on the lonsdaleite phases of C, Si and Ge. *J. Phys.: Condens. Matter* **2003**, *15*, L197−L202.

(13) Yeh, C.-Y.; Lu, Z. W.; Froyen, S.; Zunger, A. Zinc-blende \wurtzite polytypism in semiconductors. *Phys. Rev. B: Condens. Matter Mater. Phys.* **1992**, *46*, 10086.

(14) Caroff, P.; Dick, K. A.; Johansson, J.; Messing, M. E.; Deppert, K.; et al. Controlled polytypic and twin-plane superlattices in III-V nanowires. *Nat. Nanotechnol.* **2009**, *4*, 50−55.

(15) Johansson, J.; Karlsson, L. S.; Svensson, C. P. T.; Martensson, T.; Wacaser, B. A.; et al. Structural properties of < 111 > B-oriented III−V nanowires. *Nat. Mater.* **2006**, *5*, 574−580.

(16) Priante, G.; Harmand, J.-C.; Patriarche, G.; Glas, F. Random stacking sequences in III-V nanowires are correlated. *Phys. Rev. B: Condens. Matter Mater. Phys.* **2014**, *89*, 241301.

(17) Mohan, P.; Motohisa, J.; Fukui, T. Controlled growth of highly uniform, axial/radial direction-defined, individually addressable InP nanowire arrays. *Nanotechnology* **2005**, *16*, 2903−2907.

(18) Dick, K. A.; Thelander, C.; Samuelson, L.; Caroff, P. Crystal phase engineering in single InAs nanowires. *Nano Lett.* **2010**, *10*, 3494−3499.

(19) De, A.; Pryor, C. E. Predicted band structures of III-V semiconductors in the wurtzite phase. *Phys. Rev. B: Condens. Matter Mater. Phys.* **2010**, *81*, 155210.

(20) Assali, S.; Gagliano, L.; Oliveira, D. S.; Verheijen, M. A.; Plissard, S. R.; et al. Exploring Crystal Phase Switching in GaP Nanowires. *Nano Lett.* **2015**, *15*, 8062−8069.

(21) Ribeiro, E.; Govorov, A.; Carvalho, W.; Medeiros-Ribeiro, G. Aharonov-Bohm Signature for Neutral Polarized Excitons in Type-II Quantum Dot Ensembles. *Phys. Rev. Lett.* **2004**, *92*, 126402.

(22) Sellers, I.; Whiteside, V.; Kuskovsky, I.; Govorov, A.; McCombe, B. Aharonov-Bohm excitons at elevated temperatures in Type-II ZnTe/ZnSe quantum dots. *Phys. Rev. Lett.* **2008**, *100*, 136405.

(23) Bansal, B.; Hayne, M.; Geller, M.; Bimberg, D.; Moshchalkov, V. Excitonic Mott transition in type-II quantum dots. *Phys. Rev. B: Condens. Matter Mater. Phys.* **2008**, *77*, 241304.

(24) Barceló, I.; Guijarro, N.; Lana-Villarreal, T.; Gómez, R. *Quantum dot solar cells*; Springer: New York, 2014; Chapter 1.

(25) Luque, A.; Linares, P. G.; Mellor, A.; Andreev, V.; Marti, A. Some advantages of intermediate band solar cells based on Type II quantum dots. *Appl. Phys. Lett.* **2013**, *103*, 123901.

(26) Kim, S.; Lim, Y. T.; Soltesz, E. G.; De Grand, A. M.; Lee, J.; et al. Near-infrared fluorescent Type II quantum dots for sentinel lymph node mapping. *Nat. Biotechnol.* **2004**, *22*, 93−97.

(27) Konstantatos, G.; Sargent, E. H. Nanostructured materials for photon detection. *Nat. Nanotechnol.* **2010**, *5*, 391−400.

(28) Benson, O.; Santori, C.; Pelton, M.; Yamamoto, Y. Regulated and entangled photons from a single quantum dot. *Phys. Rev. Lett.* **2000**, *84*, 2513−2516.

(29) Chauvin, N.; Hadj Alouane, M. H.; Anufriev, R.; Khmissi, H.; Naji, K.; et al. Growth temperature dependence of exciton lifetime in wurtzite InP nanowires grown on silicon substrates. *Appl. Phys. Lett.* **2012**, *100*, 011906.

(30) Perinetti, U.; Akopian, N.; Samsonenko, Y. B.; Bouravleuv, A. D.; Cirlin, G. E.; et al. Sharp emission from single InAs quantum dots grown on vicinal GaAs surfaces. *Appl. Phys. Lett.* **2009**, *94*, 2009−2011.

(31) De Godoy, M. P. F.; Gomes, P. F.; Nakaema, M. K. K.; Iikawa, F.; Brasil, M. J. S. P.; et al. Exciton g factor of type-II InP GaAs single quantum dots. *Phys. Rev. B: Condens. Matter Mater. Phys.* **2006**, *73*, 033309.

(32) Matsuda, K.; Nair, S. V.; Ruda, H. E.; Sugimoto, Y.; Saiki, T.; et al. Two-exciton state in GaSb/GaAs type II quantum dots studied using near-field photoluminescence spectroscopy. *Appl. Phys. Lett.* **2007**, *90*, 013101.

(33) Van Weert, M. H. M.; Akopian, N.; Kelkensberg, F.; Perinetti, U.; Van Kouwen, M. P.; et al. Orientation-dependent optical-polarization properties of single quantum dots in nanowires. *Small* **2009**, *5*, 2134−2138.

(34) Ba Hoang, T.; Moses, A. F.; Ahtapodov, L.; Zhou, H.; Dheeraj, D. L.; et al. Engineering parallel and perpendicular polarized photoluminescence from a single semiconductor nanowire by crystal phase control. *Nano Lett.* **2010**, *10*, 2927−2933.

(35) Bayer, M.; Ortner, G.; Stern, O.; Kuther, A.; Gorbunov, A.; et al. Fine structure of neutral and charged excitons in self-assembled In(Ga)As/(Al)GaAs quantum dots. *Phys. Rev. B: Condens. Matter Mater. Phys.* **2002**, *65*, 1−23.

(36) Thompson, R.; Stevenson, R.; Shields, A.; Farrer, I.; Lobo, C.; et al. Single-photon emission from exciton complexes in individual quantum dots. *Phys. Rev. B: Condens. Matter Mater. Phys.* **2001**, *64*, 201302.

(37) Zhang, L.; Luo, J.-W.; Zunger, A.; Akopian, N.; Zwiller, V.; et al. Wide InP nanowires with wurtzite/zincblende superlattice segments are Type-II whereas narrower nanowires become type-I: an atomistic pseudopotential calculation. *Nano Lett.* **2010**, *10*, 4055−4060.

(38) Schliwa, A.; Winkelnkemper, M.; Lochmann, A.; Stock, E.; Bimberg, D. In(Ga)As/GaAs quantum dots grown on a (111) surface as ideal sources of entangled photon pairs. *Phys. Rev. B: Condens. Matter Mater. Phys.* **2009**, *80*, 161307.

(39) Singh, R.; Bester, G. Nanowire quantum dots as an ideal source of entangled photon pairs. *Phys. Rev. Lett.* **2009**, *103*, 063601.

(40) Ding, Y.; Wang, X. D.; Wang, Z. L. Phase controlled synthesis of ZnS nanobelts: zinc blende vs wurtzite. *Chem. Phys. Lett.* **2004**, *398*, 32−36.

(41) Shan, C. X.; Liu, Z.; Zhang, X. T.; Wong, C. C.; Hark, S. K. Wurtzite ZnSe nanowires: growth, photoluminescence, and single-wire Raman properties. *Nanotechnology* **2006**, *17*, 5561−5564.

DOI: 10.1021/acs.nanolett.5b04217
Nano Lett. 2016, 16, 1081−1085

Supplementary Information

Photon Cascade from a Single Crystal Phase Nanowire Quantum Dot

Maaike Bouwes Bavinck, Klaus D. Jöns, Michal Zieliński, Gilles Patriarche,

Jean - Christophe Harmand, Nika Akopian, and Val Zwiller

Supp. Information 1 – Polarization for optical transitions of Figure 1d).

Figure S1 shows the polarization for the transitions labeled X and XX in Figure 1d). We determine the polarization by performing Stokes measurements. We measure the spectrum in six different bases: the linear polarization along (z) and perpendicular to the nanowire, diagonal and anti-diagonal, and the left and right circular components. The analyzed data is shown in
Figure S1 together with the direction of the nanowire. We observe a strong linear component along the nanowire for both the X and XX transitions.

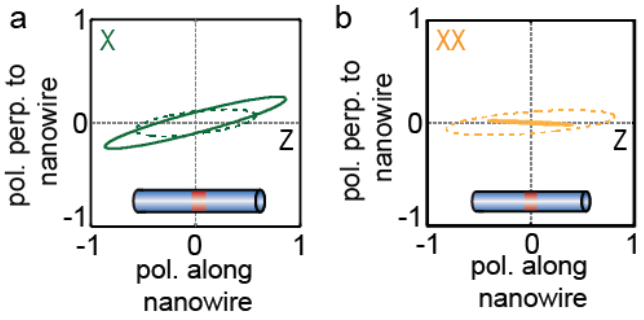

Figure S1. The polarization for the transition shown in Figure 1d) are strongly polarized along the nanowire for X (a) and XX (b).

Supp. Information 2 – Additional spectra

In Figure S2 we show additional spectra of crystal phase quantum dots in four different nanowires.

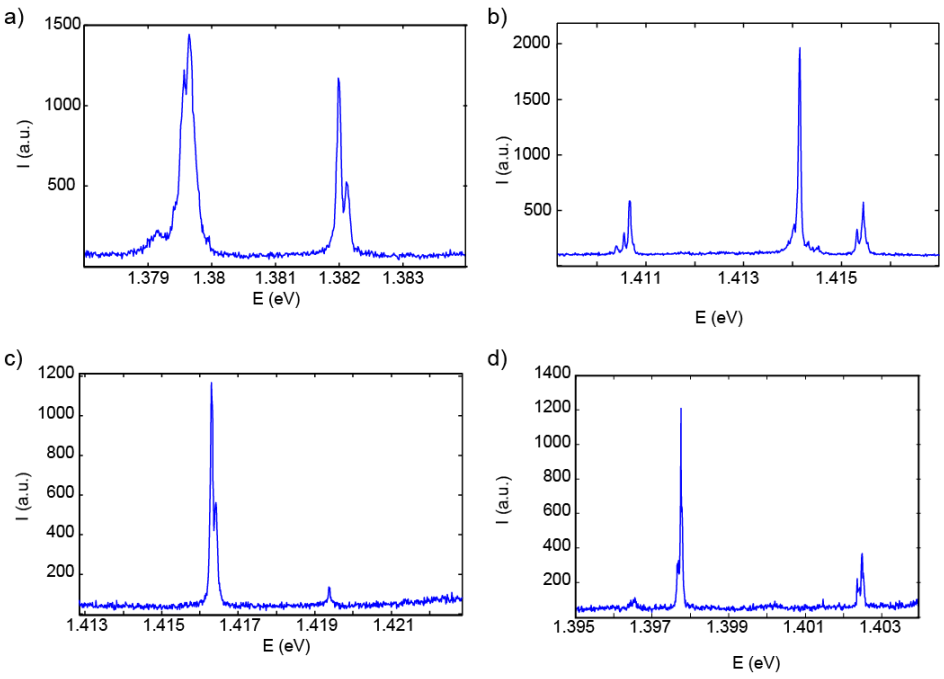

Figure S2. Four additional spectra from crystal phase quantum dots measured on different nanowires. All spectra show the double peak feature similar to the quantum dots measured in the main text and predicted by our calculations.

Supp. Information 3 - Theoretical Calculations - Methods

We use empirical tight-binding theory for the electron and hole states with an *sp3s** orbital model and nearest neighbors coupling. For the zinc blende InP section, we use Vogl et al.[1] tight-binding parameters augmented to account for spin-orbit effects. For the wurtzite InP section, we have additionally modified the parameters from Vogl et. al.[1] to account for the increased band-gap and the valence band offset between the wurtzite and zinc blende segments. We model the quantum dots by a zinc blende InP segment of height $(ZB)_n$, where n is number of (ABC) stacks, along the [111] direction embedded between two wurtzite InP segments along [0001] direction. The electronic structure calculation for different crystal polytypes is still an active field of research[2]. We fit our tight-binding parameters to reproduce the wurtzite band gap (1.474 eV), and the wurtzite-zinc blende valence band offset (64.6 meV) as has been recently reported by De and Pryor[2]. The zinc blende band gap is set to 1.41 eV. The spin-orbit splitting is assumed to be identical in the zinc blende and wurtzite crystal phases and is equal to 126 meV.

The crystal field splitting in wurtzite induces a relatively small splitting of A and B bulk hole bands. Unfortunately, this parameter is not reliably known, leading effectively to A-B splitting varying from 16 to over 70 meV[3,2], depending on the choice of the crystal field splitting parameter. Similarly, zinc blende/wurtzite lattice mismatch is reported in a wide range of values from 0.2% to over 1.0%[4,5]. With the zinc blende lattice constant being somewhat larger than that of wurtzite, lattice mismatch would in principle induce small tensile strain in the wurtzite region, that would act on the A-B splitting in opposite way to crystal field splitting effect. As neither strain parameters nor crystal field splitting are reliably know for wurtzite InP phase, in this work we decided to neglect both effects systematically. However, we checked that for different values of crystal field splitting and the inclusion of this effect, the excitonic emission energies changed well below 1 meV. Additionally, using zinc blende InP band deformation potentials, we estimate that strain at the interface between zinc blende and wurtzite would have effect on the energy spectra limited to several meV's.

Once the tight-binding Hamiltonian is established, we calculate the single particle spectra. We use the Hamiltonian matrix sparsity and calculate several lowest electron and hole states. The appearance of a free surface leads to the existence of spurious surface states due to dangling

bonds. We shift the dangling bond energies to shift the energies of surface-localized states away from the energies corresponding to the wurtzite/ zinc blende InP band gap region. We assume the wurtzite segments lengths to be equal to 30 nm (100 monolayers), resulting in a total domain height of more than 60 nm. This dimension is consistent with the experimentally observed density of zinc blende sections (15 segments/μm), i.e. ~60 nm per entire wurtzite-zinc blende-wurtzite system. The single particle computation is than followed by a configuration interaction method[3] for many-body states calculation and to obtain the excitonic optical (absorption) spectra. A calculation for the largest diameter system containing about 5 million atoms is the limit of what can be calculated with available computational resources.

Supp. Information 4 – Electron and hole states

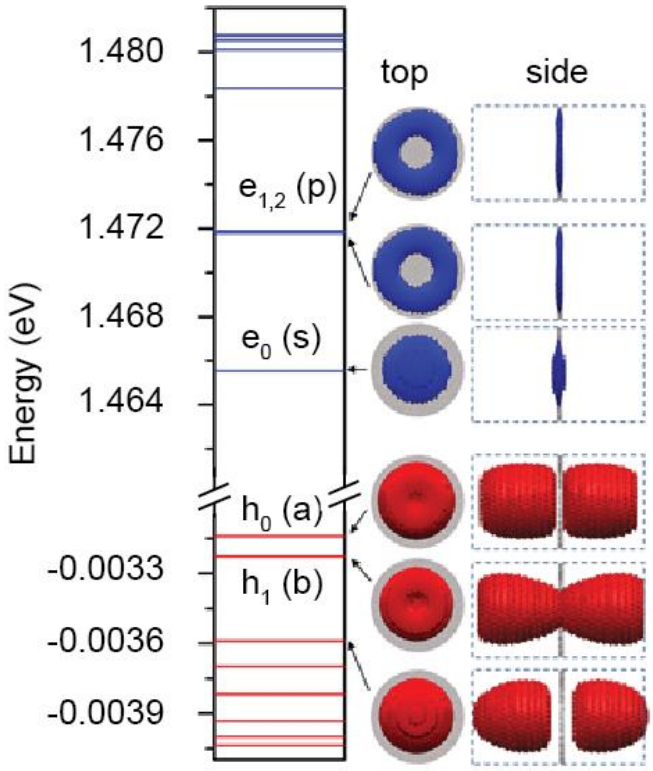

Figure S3. Single particle energies (left) and the corresponding charge densities for several lowest electron (up/blue) and hole (down/red) states in a crystal phase quantum dot system built from a single zinc blende section of height $(ZB)_1$

Figure S3 shows the single particle energies and the corresponding charge densities for several lowest electron and hole states in a crystal phase quantum dot system built form a single zinc blende sequence, $(ZB)_1$, embedded into a wurtzite nanowire of 32 nm diameter. The left isosurface plot (electron density of $3 \cdot 10^{-4}$ and hole $2 \cdot 10^{-5}$ densities) in the figure corresponds to a view along the nanowire growth axis and the plot on the right shows the isosurface along the nanowire. The single particle structure of the confined electron states in the zinc blende segment closely resembles that of self-assembled or nanowire quantum dots. The ground electron state is of s-like character, whereas the first and second excited electron states are of p-like character, with small (~0.1 meV) p-shell splitting due to the quantum dot symmetry (C_{3v}). The higher

electron states are delocalized over the nanowire. The spacing between the s- and p-electron states is 6.3 meV and is much smaller than in e.g. InAs/InP nanowire quantum dots. This is due to the shallow electron confining potential of the wurtzite – zinc blende conduction band offset (129 meV) and the reduced lateral confinement because of the relatively large nanowire diameter. The single particle hole states are very different from the electron states. They are delocalized over the wurtzite part of the nanowire and the energy spacing between subsequent hole states are small due to reduced confinement in wurtzite sections. The ground (h_0) and the first excited (h_1) hole states form a pair of closely energetically spaced states, separated only by 88 μeV. The first excited hole states is further separated by 360 μeV from the higher excited hole states.
The hole states localized in the left and right wurtzite sections of the nanowire are coupled via the zinc blende barrier to form an anti-bonding state (ground hole state) and a bonding state (excited hole state) delocalized over the entire system. The dipole moment between the ground hole state and ground electron state is about four orders of magnitude weaker than the dipole moment between the first excited hole state and the ground electron state.

With increasing nanowire diameter, the overall single particle properties remains unaltered, however, the inter-level energy differences are significantly reduced. For a nanowire with a diameter of 48 nm the spacing between s-like and p-like electron states is 3 meV and the p-shell splitting is only 25 μeV. The difference between h_0 and h_1 is 19 μeV, whereas h_2-h_1 spacing is only 63 μeV. The reduces inter-level spacing will lead to significant configuration mixing.

The single particle configuration is then followed by many-body (configuration interaction, exact diagonalization) calculation. Due to computational limits, in this calculation we include three lowest electron states (6 with spin), what effectively corresponds to accounting for electron and s- and p-shells. On the hole side we include 4 lowest (8 with spin) states. Therefore we account for 48 configurations to solve the single exciton problem, and 480 configurations for the biexciton.

Supp. Information 5 – Z and x/y polarization for different diameter and different crystal phase quantum dot configurations.

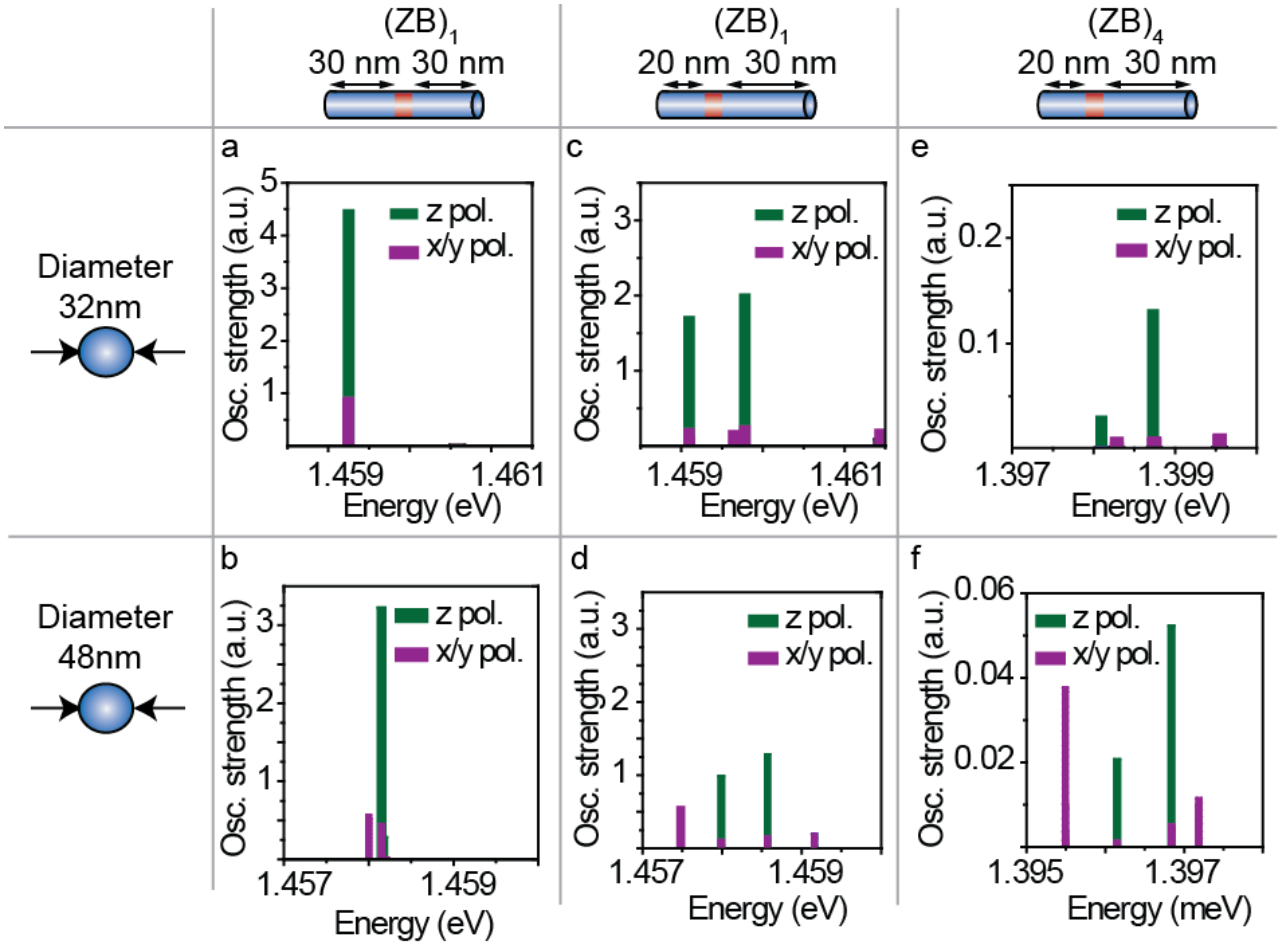

Figure S4. Calculations for different crystal phase quantum dot configurations. For two different diameters we show the results for a zinc blende section of size $(ZB)_1$ incorporated in a symmetric ((a) and (b)) and asymmetric wurtzite matrix ((c) and (d)). Figure (e) and (f) show a zinc blende section of $(ZB)_4$ in an asymmetric wurtzite matrix.

In Figure S4 we summarize our results of the calculations for different crystal phase quantum dot systems. We performed detailed calculations for two different nanowire diameters 32 nm and 48 nm. One can extract from the figures different trends. For a zinc blende section of $(ZB)_1$ in a symmetric matrix one observes a single peak for z-polarized light. When breaking the symmetry of the wurtzite matrix, the peak is split into two peaks. This is also the case for larger zinc blende structures ($(ZB)_4$), however, the overall oscillator strength is lower. For x/y-polarized lines, the intensity is weaker than the z-polarized transition, except for Figure S4f), where the z-polarized

and x/y-polarized lines are of the same strength. Also, we notice that the oscillator strength for all transitions decreases for increasing diameter.

Supp. Information 6 – Lifetime

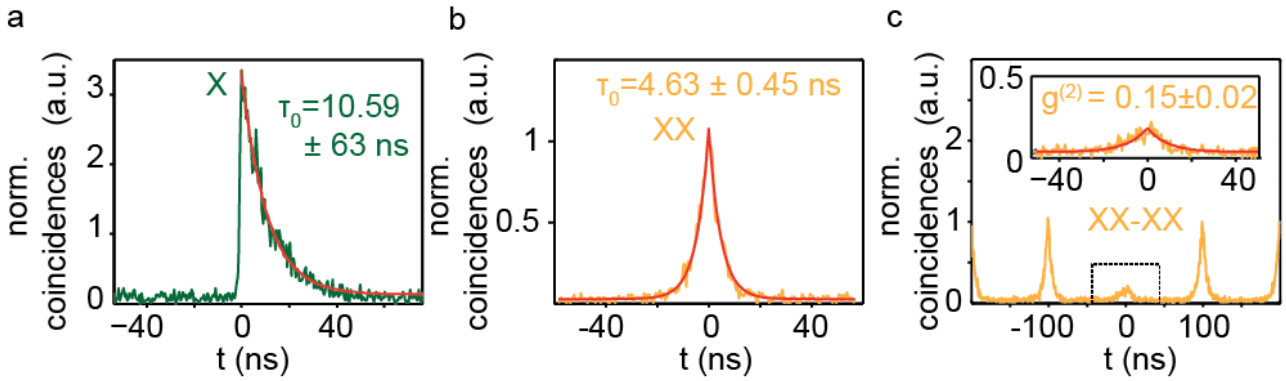

Figure S5. The measured and fitted lifetime for the (a) exciton and (b) biexciton. Figure (c) shows the fit to extract the g_2 value from the biexciton.

Figure S5 shows the fits that we used to extract the lifetimes and $g^{(2)}(0)$. To extract the lifetime of the exciton we use the cross-correlation measurements (Figure S5a)) and we use the auto-correlation measurement of the biexciton for the biexciton lifetime (Figure S5b)). We fit the data with a single exponential: $N(t) = A\left(1 - e^{\left|\frac{t-t_0}{\tau_0}\right|}\right)$, where A and t_0 are fitting parameters and τ_0 is the lifetime. For the exciton we extract a lifetime of 10.59 ± 0.63 ns and for the biexciton a lifetime of 4.63 ± 0.45 ns. We fit the antibunching peak of the biexciton (Figure S5c)) to extract a $g^{(2)}(0)$ of 0.15± 0.02. We observe a small dip at t = 0 ns indicating possible re-excitation of the quantum dot.

References

(1) Vogl, P., Hjalmarson, H. P. , & Dow, J.. *J. Phys. Chem. Solids* **1983**, *44*, 365.

(2) De, A. & Pryor, C. E.. *Phys. Rev. B* **2010**, *81*, 155210

(3) Zhang, L., Luo, J.-W., Zunger, A., Akopian, N., Zwiller, V., & Harmand, J.-C. *Nano Lett.* **2010**, *10*, 4055.

(4) Kriegner, D., Wintersberger, E., Kawaguchi, K., Wallentin, J., Borgström, M.T., & Stangl, J. Nanotechnology **2011**, *22*, 425704.

(5) Dacal, L. C. O. & Cantarero, A. Solid State Commun. **2011**, *151*, 781.

(6) Zielinski, M., Korkusinski, M., & Hawrylak, P. Phys. Rev. B **2010**, *81*, 085301.